ACS Sustainable Chemistry & Engineering

Research Article

pubs.acs.org/journal/ascecg

A ^{31}P NMR and TG/DSC-FTIR Investigation of the Influence of Initial pH on Phosphorus Recovery as Struvite

Ning Ma,[†,‡] Ashaki A. Rouff,*[,†,‡] and Brian L. Phillips[§]

[†]School of Earth and Environmental Sciences, Queens College, City University of New York, Queens, New York 11367-1597, United States

[‡]Earth and Environmental Sciences Doctoral Program, The Graduate Center, City University of New York, New York, New York 10016-4309, United States

[§]Department of Geosciences, Stony Brook University, Stony Brook, New York 11794-2100, United States

Supporting Information

ABSTRACT: Phosphorus can be reclaimed from nutrient-rich sources as the mineral struvite ($MgNH_4PO_4 \cdot 6H_2O$) for reuse as fertilizer. This study determines the impact of initial pH (pH_i) from 8 to 11 on the fraction of precipitated struvite from a $MgCl_2-(NH_4)_2HPO_4-NaCl-H_2O$ system. The rate of P removal from solution increases with pH_i and maximizes at pH_i 10. Scanning electron microscopy (SEM) of recovered precipitates shows changes in morphology and decreasing particle size with increasing pH_i. ^{31}P nuclear magnetic resonance spectroscopy (NMR) confirms that struvite constitutes 96−99% of the phosphate at pH_i 8−10, with newberyite ($MgHPO_4 \cdot 3H_2O$) as a minor crystalline phase. At pH_i 11, 60% of the solid is struvite, with 22% of the phosphate contained in an amorphous phase and 18% as sodium phosphate. Thermogravimetric analysis (TG) reveals a correlation in the mass loss from the solids with the percentage of struvite detected. Coupling Fourier transform infrared spectroscopy (FT-IR) with TG indicates that the molar concentration of evolved $H_2O(g)$ and $NH_3(g)$ is influenced by the adsorption of $NH_4^+(aq)$ at pH_i 8−10 and by the low percentage of struvite at pH_i 11. Overall, results indicate that both the amount of P recovered and the fraction of struvite are optimized at pH_i 10. These findings can be used as a starting point in the selection of a suitable pH_i for struvite recovery from nutrient-rich wastes.

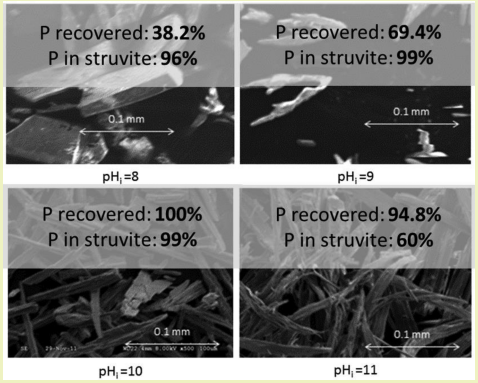

KEYWORDS: *P fertilizer, P sustainability, P recovery, P NMR, Simultaneous thermal analysis, Struvite, Wastewater*

INTRODUCTION

Geologic phosphorus (P) reserves are currently being depleted, decreasing the supply of P for agricultural purposes, with implications for global food security.[1] The recovery of P from nutrient-rich wastes could simultaneously lessen the burden on geologic P reserves and provide an additional source of P to address an increasing global demand.[2] The mineral struvite ($MgNH_4PO_4 \cdot 6H_2O$) can be precipitated from urine and animal, plant, and municipal wastes[3−5] to recover P from these sources. Struvite may in turn be a viable fertilizer due to the high P and nitrogen (N) content. In addition, the low solubility of struvite means that it can be used as a slow-release fertilizer, providing nutrients to plants and crops over an extended period.[6] Struvite-based fertilizers synthesized from different types of nutrient-rich wastes are already being promoted as commercial fertilizers.[7]

pH_i is the initial pH to which the P-rich waste is adjusted in order to induce P removal. This is of significance as in some cases pH is not controlled or maintained throughout the recovery process.[2,4] Therefore, the pH_i is one of the most important factors that can affect the rate of struvite crystallization and the chemical and physical properties of the mineral when precipitated from solution. The change in the concentration of total dissolved orthophosphate (PO_4-P) can be used to monitor the rate of precipitate (mainly struvite) formation. Using this approach, the nucleation, crystal growth, and precipitation of struvite were found to follow a first-order kinetics model with respect to PO_4-P concentration.[8−10] The crystal growth rate was found to be transport controlled[11] and dependent on the second order of the concentration of PO_4-P.[12] It has also been proposed that the growth rate may follow a two-step linear model.[13] The pH_i of the solution can be used to determine the coefficients in the kinetic equations.[13] The pH_i can also dictate the supersaturation[14] and nucleation rate of struvite from solution, but it may have a minor effect on the crystal growth rate.[11]

The pH_i can also affect the morphology, particle size, and thermal properties of struvite. Struvite has an orthorhombic unit cell in space group $Pmn2_1$;[15] however, the shape and size of crystals can vary with pH_i. For example, in the presence of

Received: November 14, 2013
Revised: January 10, 2014
Published: January 13, 2014

   dx.doi.org/10.1021/sc4004746 | ACS Sustainable Chem. Eng. 2014, 2, 816−822

acetate, dendritic, elongated dendritic, and needle-shaped crystals were observed to form at pH_i 7, 7.5, and 10, respectively.[16] For struvite crystallized between pH_i 7−11, smaller crystals were observed at pH_i 9−10 compared to the lower pH_i values.[3] These physical changes, as well as potential changes in the chemical properties and composition of struvite with pH_i, could also impact the thermal properties of the mineral. The mineral phase transitions during the thermal decomposition of struvite have been studied extensively.[17−19] It is also known that the presence of impurities can impact these processes.[20] However, the effect of pH of crystallization on the thermal properties of struvite, especially the release of volatile components during the heating process, has not been previously determined. The thermal properties can be used to assess the relative stability of struvite when generated at different pH_i. Although these experiments are conducted at above ambient temperature, this provides an initial assessment of the susceptibility of struvite to decomposition and thus the release of nutrients when used as a fertilizer.

The purity of struvite with respect to additional mineralogical components and the association of contaminants can also be influenced by pH_i. In batch experiments conducted over a pH_i range of 7−10, the pH was found to be the primary factor affecting the production of struvite.[21] At pH_i 6−9, 39% hydroxylapatite ($Ca_5(PO_4)_3OH$) and 5−55% newberyite ($MgHPO_4{\cdot}3H_2O$) were detected separately along with struvite in solids precipitated from wastewater.[22,23] Trace components in solution can also associate with struvite during mineral formation, resulting in impurities in the recovered precipitate.[14,24] This has been observed for struvite formation in the presence of As, where increasing the pH_i over a range of 8−10 also increased the As content of the recovered solid.[14]

This study focuses on the impact of pH_i 8−11, a range typical for optimal struvite formation,[9,21] on the physical and chemical properties of struvite precipitated from a $MgCl_2$−$(NH_4)_2HPO_4$−NaCl−H_2O system. The system was chosen to provide fundamental information concerning the effect of pH_i on struvite formation without the influence of additional ions present in more complex solutions. The pH_i was fixed, and the overall pH of the system was allowed to drift with the removal of P until equilibrium was reached. These conditions are similar to those used for struvite recovery from urine and wastewater, where the pH is difficult to control due to economical and/or technical reasons, for example, in rural areas of third world countries.[3,9,23,25] The morphology, mineralogy, and thermal behavior of the solids recovered from these solutions were determined. Findings from ^{31}P nuclear magnetic resonance spectroscopy (NMR) and simultaneous thermal analysis coupled with Fourier transform infrared spectroscopy (TG/DSC-FTIR) provide new insight into the influence of pH_i on struvite formation. In turn, an improved fundamental understanding of the impact of pH_i on the physical properties and chemical composition of precipitates from struvite-saturated solutions is necessary to ultimately improve the recovery of P from nutrient-rich wastes.

MATERIAL AND METHODS

Preparation of Struvite-Saturated Solutions. Solutions of $MgCl_2{\cdot}6H_2O$ and $(NH_4)_2HPO_4$ were prepared in deionized water at room temperature (~20−22 °C) in HDPE bottles. A NaCl electrolyte was used to maintain the ionic strength of the solutions at 0.1 M. Commercial struvite (Alfa Aesar) was added to the $(NH_4)_2HPO_4$ solution at a loading of 0.1 g/L to overcome the initial energy barrier, decrease the induction time associated with nucleation, and optimize the crystallization of struvite during precipitation.[26,27] An equimolar concentration of $MgCl_2{\cdot}6H_2O$ was mixed with the $(NH_4)_2HPO_4$ solution so that the concentration of reagents was 17 mM. The pH_i was adjusted to 8, 9, 10, or 11 using a 2 N NaOH solution.

The initial saturation index of struvite ($SI_{struvite}$) prior to pH adjustment was calculated to be ~2 using the program PHREEQC[28] with the minteq.v4 database, and the struvite solubility product ($K_{sp\ struvite}$) from the literature at $10^{-13.26}$.[29] The $SI_{struvite}$ can be described by the following equations

$$SI_{struvite} = \log_{10}[IAP_{struvite}/K_{sp\ struvite}] \quad (1)$$

$$IAP_{struvite} = a_{Mg^{2+}} \times a_{NH_4^+} \times a_{PO_4^{3-}} \quad (2)$$

$$K_{sp\ struvite} = 10^{-13.26} \quad (3)$$

where $IAP_{struvite}$ is the ion activity product of participating aqueous species.[14] For pH_i 8−11, the $SI_{struvite}$ was calculated to be 2.18, 3.05, 3.42, and 3.11, respectively. The decrease in $SI_{struvite}$ at pH_i 11 was due to the decrease in the activity of Mg^{2+}(aq) and NH_4^+(aq). The SI of other P-bearing minerals was also calculated by PHREEQC for each pH_i (Table S1, Supporting Information).

Phosphorus Removal from Solution. Solutions with an initial PO_4−P concentration of 17 mM were prepared as described above at pH_i 8−11. Immediately after mixing the $MgCl_2{\cdot}6H_2O$ and $(NH_4)_2HPO_4$ solutions, the pH was adjusted, and a small volume of solution was retrieved and filtered using 0.45 μm syringe filters. Filtered aqueous samples were retrieved intermittently over a 24 h reaction time. All aqueous samples were acidified with 6 M HCl immediately after sampling and analyzed for total dissolved orthophosphate (PO_4−P) by a Lachat QuikChem 8000 nutrient analyzer using ascorbic acid method 31-115-01-1 for orthophosphate. The detection limit for this technique is 0.01 mg P/L, and major interferents such as iron and silica were not present in solution.

Synthesis and Characterization of Solids. Solids were synthesized at pH_i 8−11 using the approach described above. After a 24 h reaction period, the solids were recovered by filtering the entire solution volume using 0.22 μm filters. Recovered solids were allowed to dry at room temperature prior to subsequent analysis.

The morphology of the solids was determined by scanning electron microscopy (SEM) of carbon-coated solids using a Hitachi S-2600N instrument. Powder X-ray diffraction (XRD) patterns of the solids were collected using a Philips X'Pert Pro instrument. Data were collected using Cu Kα radiation over a range of 10−40° 2θ, with a counting time of 1 s for every 0.01°. The diffraction patterns were background corrected and analyzed using X'Pert Highscore from PANalytical B.V. Where necessary, unanticipated phases detected by XRD were further investigated. In this case, the solids were digested in 5% HNO_3 and analyzed for major cations by inductively coupled plasma optical emission spectroscopy (ICP-OES) using a Perkin-Elmer DV 5300.

Nuclear magnetic resonance (NMR) spectroscopy was used to determine the identity of P-bearing phases in the precipitates. The ^{31}P MAS/NMR spectra were acquired with a 500 MHz Varian Infinity-plus spectrometer operating at 202.3 MHz for ^{31}P. Samples were contained in 4 mm rotors (o.d.) spinning at 8 kHz. Quantitative spectra were acquired by direct excitation with 4 μs pulses ($\pi/2$) and 120 s relaxation delays to allow complete relaxation with high-power ^1H decoupling during acquisition. The ^{31}P chemical shifts are reported relative to 85% H_3PO_4(aq) using hydroxylapatite as a secondary standard set to 2.65 ppm.

The thermal properties of the solids were determined by simultaneous thermal analysis using thermogravimetry (TG) and differential scanning calorimetry (DSC). Fourier transform infrared spectroscopy (FT-IR) was used to identify and quantify the H_2O(g) and NH_3(g) released from the solids during thermal decomposition. For these analyses, a Perkin-Elmer STA 6000 simultaneous thermal analyzer was connected to a Spectrum 100 FT-IR spectrometer by a gas transfer line and a dedicated FT-IR cell. About 20 mg of solid was

dx.doi.org/10.1021/sc4004746 | ACS Sustainable Chem. Eng. 2014, 2, 816−822

placed in a ceramic crucible and heated at a rate of 10 °C/min over a range of 35−500 °C. Dry N_2 gas was used to purge the sample at a flow rate of 20 mL/min. Evolved gases were transported through the transfer line into the FT-IR cell, both of which were heated to 250 °C to prevent gas condensation. The FT-IR was programmed to collect background-corrected spectra continuously over a range of 650−4000 cm^{-1} wavenumbers for the duration of the heating program. The areas of the peaks assigned to $H_2O(g)$ and $NH_3(g)$ in the FT-IR spectra were calculated. This was combined with the mass loss from the TG curve to quantify the molar concentrations of $H_2O(g)$ and $NH_3(g)$ evolved.

RESULTS AND DISCUSSION

Phosphorus Removal from Solution. At all pH_i values, the concentration of PO_4−P in solution decreased dramatically in the first 2 h and gradually leveled off over the 24 h period (Figure 1). The final measured pH values (pH_f) are consistent

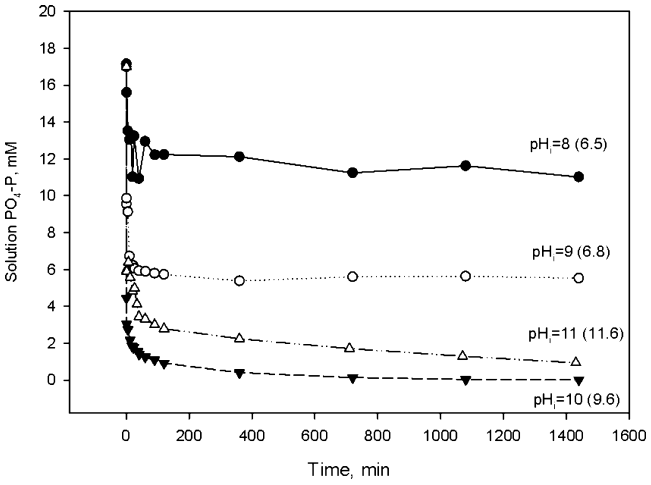

Figure 1. PO_4−P concentrations in solution during solid precipitation at pH_i 8−11 over a 24 h period. The final pH in solution is indicated in brackets.

with those predicted by thermodynamic calculations using PHREEQC (Table S1, Supporting Information) and are indicative of equilibrium. Starting with an initial concentration of 17 mM PO_4−P, the final concentrations at pH_i 8−11 are 10.5, 5.2, 0.01, and 0.89 mM PO_4−P, respectively. This result indicates enhanced removal of P from solution as pH_i is increased, with maximum removal at pH_i 10. This trend correlates well with the $SI_{struvite}$ at the onset of precipitation, which indicates the impact of $SI_{struvite}$ and pH_i on the efficiency of P removal. Besides the influence of $SI_{struvite}$ on the final PO_4−P concentration, this parameter also affects the rate of PO_4−P removal. As seed material is added to overcome the nucleation energy, significantly reducing the induction time, the primary effect of high $SI_{struvite}$ values is to impact the rate of precipitation and thus P removal from solution. Because of this, a more pronounced reduction in the concentration of PO_4−P occurs at the beginning of the reaction, within 1−2 h of the onset of precipitation, at higher pH_i as shown in Figure 1. At pH_i 10, where $SI_{struvite}$ is the highest, the rate of removal and also the concentration of PO_4−P removed from the aqueous phase are maximized. This is consistent with previous results that indicated that the mass of recovered solid was highest at pH_i 10, with a yield of 4.1 g/L compared to 1.0 g/L at pH_i 8.[14]

Scanning Electron Microscopy. The SEM images of single crystals recovered from pH_i 8−11 solutions show distinct morphologies at different pH_i values (Figure 2a−d). At pH_i 8, the crystals are well-formed blocky crystals indicative of orthorhombic symmetry and consistent with struvite synthesized from pH_i 5−8 in previous studies.[30,31] At pH_i 9, the crystals are elongated and bar shaped, whereas at pH_i 10 and 11, the crystals are thinner and flatter. At pH_i 11, these thinner crystals were susceptible to curling due to surface tension of water while drying. As stated above, the rate of PO_4−P removal from solution is contingent upon pH_i. Therefore, the increased rate of precipitation at higher pH_i would decrease the PO_4−P concentration dramatically. At the same time, because the growth rate of the crystals is controlled by diffusion and/or physical mixing,[9] this rapid reduction in PO_4−P would subsequently limit the growth of crystals. Therefore, it is likely that the rapid precipitation at higher pH_i reduced the PO_4−P concentration limiting subsequent crystal growth and producing the thin flat tablet-shaped crystals observed in the SEM.

X-ray Diffraction. The XRD patterns indicate that struvite is the dominant phase precipitated from solutions with initial pH_i 8−11 (Figure 3a). For the solids formed at pH_i 8−10, the peaks from the XRD patterns show characteristic reflections of struvite. However, due to variations in the preferred orientation and particle size, the intensity of peaks varied, and not all of the reflections associated with struvite are evident in the XRD patterns. For precipitates formed at pH_i 11, characteristic reflections of both struvite and a hydrated sodium phosphate ($Na_3PO_4{\cdot}0.5H_2O$) are identified (Figure 3b). The presence of Na in solids precipitated at pH_i 11 but not at pH_i 8−10 was confirmed by ICP-OES analysis of acid-digested solids.

Nuclear Magnetic Resonance Spectroscopy. Results from ^{31}P NMR confirm that struvite dominates the precipitates at all pH_i values (Table 1 and Figure 4). The ^{31}P MAS/NMR spectra of all samples contain a prominent narrow peak at a chemical shift of +6.0 ppm that can be assigned to struvite.[32] In addition, the samples prepared at pH_i 8−10 contain a small narrow peak at −7.8 ppm near the position reported previously for newberyite.[33] The low intensity of this peak is consistent with the absence of newberyite in the XRD pattern. A peak occurs at a chemical shift near +8.3 ppm in the spectra of the solids precipitated at pH_i 11 that can be assigned to sodium phosphate based on the position of the chemical shift[34] and the appearance of XRD reflections consistent with this phase. The pH_i 11 precipitates also yield a broader peak centered near 1.5 ppm that likely arises from an amorphous or poorly crystalline material. On the side of the struvite peak, a small shoulder occurs near +5.0 ppm that can be attributed to kovdorskite ($Mg_2PO_4(OH){\cdot}3H_2O$) based on the similarity in the chemical shift to that of a well-crystallized specimen that gives a narrow peak at +4.7 ppm. Several other small narrow peaks are also apparent in the spectrum of the pH_i 11 precipitates but could not be assigned based on data available in the literature. The phase(s) responsible for these smaller peaks are likely present at too low a concentration to be easily identified by XRD.

The P-normalized relative proportions of each phase are determined from the integrated intensities obtained from least-squares fits of the centerband and significant spinning sidebands (not shown in Figure 4) to symmetrical peaks. The results are collected in Table 1, with uncertainties estimated from the variation in best-fit parameters with changes in subjective processing details (e.g., baseline and phase corrections) and fitted peak shapes. (These estimated uncertainties are conservative and far exceed those given by the covariance matrix using observed noise as the uncertainty in

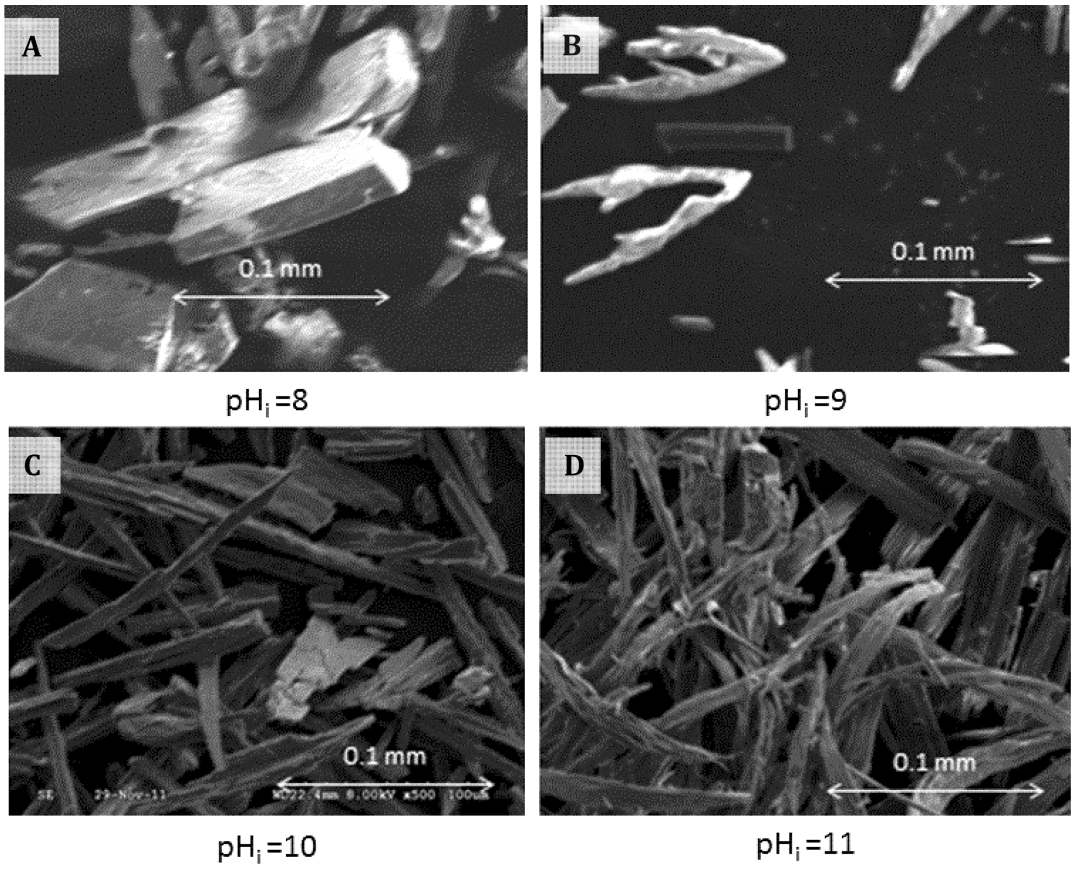

Figure 2. SEM images of solids precipitated at pH$_i$ 8−11.

spectral intensity values.) At pH$_i$ 8−10, the fraction of struvite increased from 96% at pH$_i$ 8 to ∼99% at pH$_i$ 9 and 10. At pH$_i$ 11, 60% of the P in the solid occurs in struvite. Additional phases are also identified at all pH$_i$ values. At pH$_i$ 8−10, newberyite is present as only a minor phase, the fraction of which decreased from 4% at pH$_i$ 8 to <1% at pH$_i$ 9 and 10. At pH$_i$ 11, 22% of the P is associated with an amorphous phase and 18% contained in sodium phosphate.

At pH$_i$ 8−10, the increase in the fraction of struvite in the precipitates is likely influenced by the change in SI$_{struvite}$ and the rate of precipitation with pH$_i$. Compared to pH$_i$ 8, at pH$_i$ 9−10, increased rates of struvite precipitation would limit the amount of ions, $Mg^{2+}(aq)$ and $HPO_4^{2-}(aq)$, available to form newberyite. The preferential formation of struvite is due to the lower solubility product, $K_{sp\ struvite} = 10^{-13.26}$, compared to that of newberyite, $K_{sp\ newberyite} = 10^{-5.51}$.[35] In addition, it has been reported that in the $MgCl_2-(NH_4)_2HPO_4-NaOH-H_2O$ system, the difference between the SI of struvite and that of newberyite increases as the pH$_i$ is increased[23] and is supported by results from thermodynamic calculations using PHREEQC. At pH$_i$ 11, the high rate of precipitation means that $Mg^{2+}(aq)$, $NH_4^+(aq)$, and $PO_4^{3-}(aq)$ are also removed from the solution in a short period of time. However, at this pH$_i$, the reduced activity of $NH_4^+(aq)$ would limit struvite formation, giving way to the precipitation of Mg- and Na-phosphates. Besides, given the decrease in SI$_{struvite}$, the solution chemistry at pH$_i$ 11 would be quite different from that at pH$_i$ 8−10 promoting the formation of these additional phases.

Simultaneous Thermal Analysis and Fourier Transform Infrared Spectroscopy. Results from thermal analyses are consistent with pH$_i$-induced changes in the physical properties and chemical composition of the precipitates. The primary peak in the DSC curves represents an endothermic phase transition associated with the decomposition of struvite (Figure 5). This peak shifts from 122 °C at pH$_i$ 8 to 110 °C at pH$_i$ 11, indicating that decomposition occurs at lower temperature with increasing pH$_i$. In addition, the onset point also shifts to lower temperature, from 86 °C at pH$_i$ 8 to 68 °C at pH$_i$ 11 (Figure 5). The shifts in the temperatures of the endothermic phase transition and the onset point to lower values may be due to the observed changes in the physical properties of the crystals, notably the crystal shape and size. The morphology of the crystals changes from well-formed and blocky crystals to thinner, flatter, tablet-shaped crystals as pH$_i$ is increased. In turn, the thinner crystals formed at higher pH$_i$ have a higher surface area due to their shape and size, which make them more susceptible to thermal decomposition.

The total mass loss, as shown on the TG curves (Figure 5), is highest at pH$_i$ 9−10 at 53.4−53.2%, with the lowest value of 50.8% recorded at pH$_i$ 11. The mass loss is due to the release of $H_2O(g)$ and $NH_3(g)$, as confirmed by FT-IR analysis of the evolved gases. The trend coincides well with the fraction of struvite in the solids at pH$_i$ 8−10 (Table 1) and indicates the release of more volatile components as the fraction of struvite increases. However, for the solid precipitated at pH$_i$ 11, the mass loss is not proportional to the fraction of struvite due to the presence of other phases with less volatile components relative to struvite.

The relative concentrations of $H_2O(g)$ and $NH_3(g)$ released from the solids formed at different pH$_i$ (Table 2) provide insight into the composition of the solids. The total volatile content of the solids is similar, ranging from 29.7 to 30.0

dx.doi.org/10.1021/sc4004746 | ACS Sustainable Chem. Eng. 2014, 2, 816−822

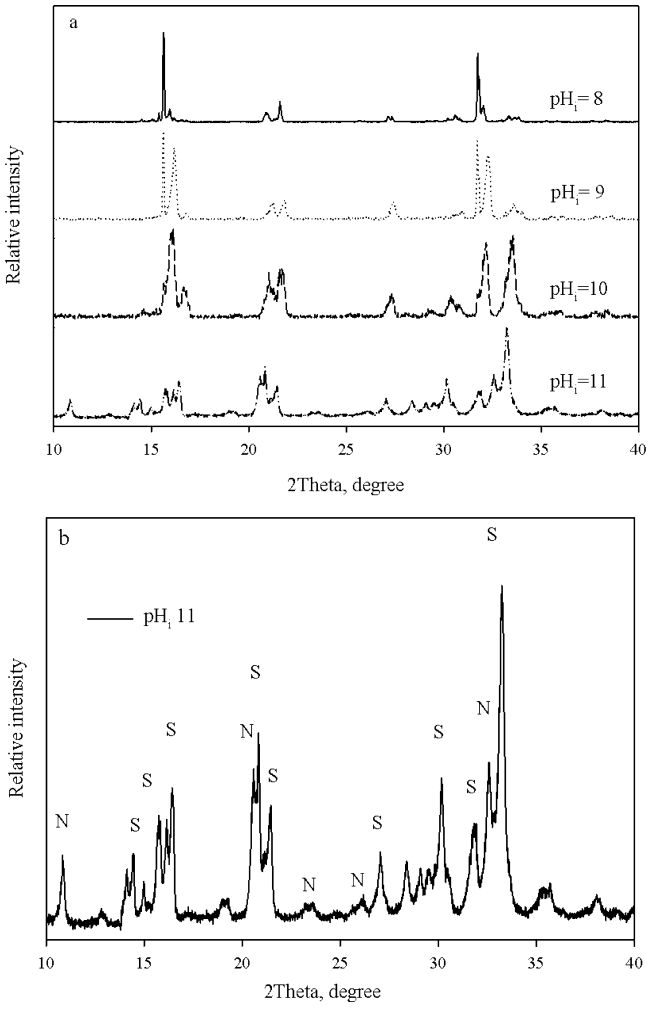

Figure 3. XRD patterns of the (a) solids precipitated at pH$_i$ 8−11 and (b) solid precipitated at pH$_i$ 11. The letters "S" and "N" represent the peaks related to struvite and sodium phosphate, respectively.

mmol/g from pH$_i$ 8−10, with a slightly lower value of 28.5 mmol/g at pH$_i$ 11. The molar ratios of $H_2O(g)$ to $NH_3(g)$ range from 1.4 to 2.5 and are lower than anticipated based on the struvite stoichiometric value, $H_2O(s)$:$NH_4^+(s)$ = 6:1, and the ratio in the literature.[20] Because the total volatile content did not change notably, the lower stoichiometric ratio between $H_2O(g)$ and $NH_3(g)$ can be interpreted as less $H_2O(s)$ and more $NH_4^+(s)$ in the solid compared to that ratio in struvite. This is probably due to the adsorption of $NH_4^+(aq)$, which is the dominant N species at pH$_i$ 8−10, to the surface of the solids. Because the surface charge of struvite becomes more negative at higher pH,[36] and the thinner smaller crystals are likely to have a higher surface area, more $NH_4^+(aq)$ could be adsorbed on the surface as the pH$_i$ was increased. The sorption

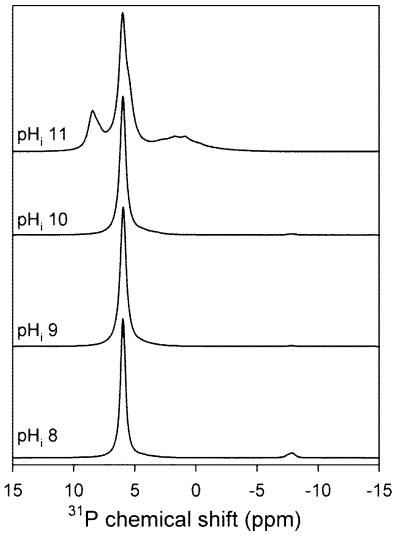

Figure 4. Quantitative ^{31}P MAS/NMR spectra of solids precipitated at the indicated pH$_i$ values. Peaks occurring at 8.3, 6, 1.5, and −7 ppm are assigned to Na-phosphates, struvite, an amorphous phase, and newberyite, respectively. Spectra were acquired by direct excitation with 120 s relaxation delays at a spinning rate of 8 kHz and represent 80 acquisitions each.

of $NH_4^+(aq)$ to struvite can be verified by determining the concentration of $NH_3(g)$ released below and above 200 °C (Table 2). On the basis of the study of the decomposition of pure struvite, the release of structural or incorporated $NH_4^+(s)$ as $NH_3(g)$ is not significant at temperatures lower than approximately 200 °C.[18] Recalculating the ratio of volatiles using only the concentration of $NH_3(g)$ released above 200 °C yields values more consistent with that expected for struvite for the pH$_i$ 8−10 solids (Table 2). Therefore, the release of $NH_3(g)$ at lower temperature is suggestive of the evolution of adsorbed $NH_4^+(aq)$ associated with the solids. The sorption of $NH_4^+(aq)$ would in turn alter the surface charge, potentially disrupting the growth of crystals, resulting in a smaller particle size at higher pH$_i$. At pH$_i$ 11, less $NH_4^+(aq)$ would be available for crystal growth due to increased formation of the neutral species, $NH_3^0(aq)$, due to hydrolysis. Also, the fraction of struvite in these solids is reduced, and additional phases are detected. So although the rate of precipitation at pH$_i$ 11 is still high, the decrease in $NH_4^+(aq)$ concentration and the formation of additional phases results in a higher ratio of $H_2O(g)$ to $NH_3(g)$ at this pH$_i$.

Impact of pH$_i$ on Struvite Formation. This study demonstrates the impact of pH$_i$ on the physical and chemical properties of struvite during its precipitation from solution. As the pH$_i$ is increased from 8 to 11, an increase in both the rate and the amount of P removal from solution were found over a 24 h period. Simultaneously, a high rate of precipitation and

Table 1. Relative Integrated Intensities of ^{31}P MAS/NMR Peaks Observed for Solids Synthesized at pH$_i$ 8−11 and Estimated Uncertainties[a]

sample	8.3 ppm $Na_3PO_4{\cdot}0.5H_2O$	6 ppm struvite	1.5 ppm (broad) amorphous phase	−7 ppm newberyite
pH$_i$ 8	n.d.	96(1)	n.d.	4(1)
pH$_i$ 9	n.d.	99.3(3)	n.d.	0.7(3)
pH$_i$ 10	n.d.	99.1(3)	n.d.	0.9(3)
pH$_i$ 11	18(2)	60(2)	22(2)	n.d.

[a]n.d. means none detected.

dx.doi.org/10.1021/sc4004746 | ACS Sustainable Chem. Eng. 2014, 2, 816−822

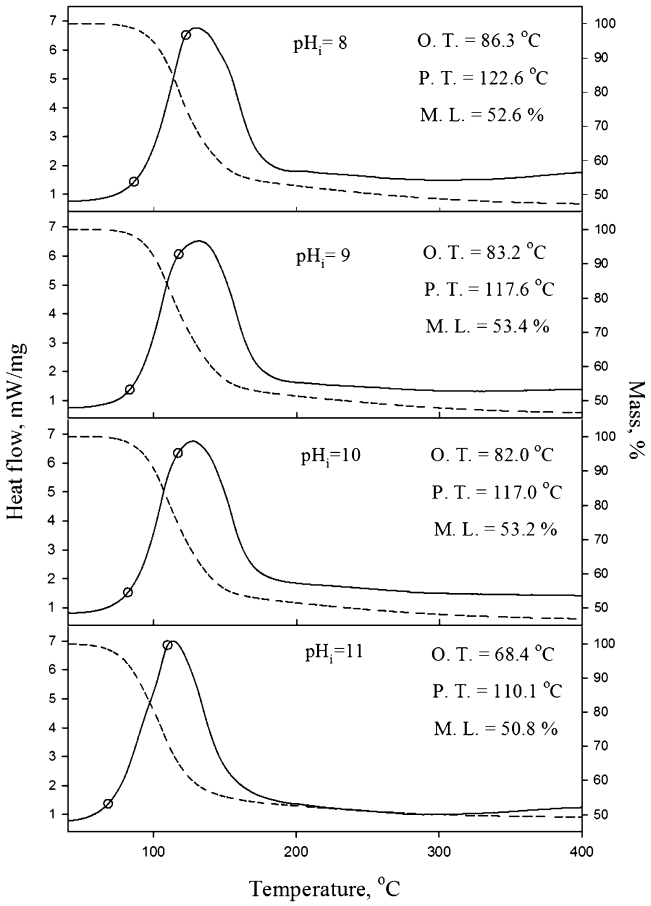

Figure 5. DSC (solid lines) and TG (dashed lines) curves for solids precipitated at pH_i 8−11. The onset temperature (O.T.) and the peak temperature (P.T.) are represented as open symbols on the DSC curve with values reported in the legend (±0.5 °C). The total mass loss (M.L.) as determined from the TG curve at 400 °C is also reported in the legend (±0.2%).

changes in aqueous speciation result in reduced concentrations of $Mg^{2+}(aq)$, $PO_4^{3-}(aq)$, and $NH_4^+(aq)$, limiting crystal growth at higher pH_i. This influences the morphology of the crystals, with the formation of thinner flatter crystals at pH_i 9−11 compared to more equant blocky crystals at pH_i 8. The fraction of different mineral phases in the solid is also affected by the pH_i. Although struvite is the dominant mineralogical phase at pH_i 8−10, a notable fraction of additional phases is detected at pH_i 11. The changes in morphology and mineralogy also affect the thermal properties of the solids, producing a shift in the temperature of decomposition to lower values at higher pH_i and affecting the total volatile content and ratio of $H_2O(s)$ to $NH_4^+(s)$ in the samples.

The results of this study have implications for the pH_i-dependent recovery of P from nutrient-rich sources, including urine and agricultural wastes. Precipitation of struvite at pH_i 8 produces large well-formed crystals that are the most thermally stable. Although the size and morphology of the crystals formed at pH_i 9−10 reduces the thermal stability, P removal from solution is higher at these pH_i values. In addition, the percentage of struvite recovered at these pH_i values is >99% of the total P. At pH_i 11, although P recovery is high, the struvite content is lower at 60%, which also signifies less efficient removal of N from solution, in addition to which the solids are the most susceptible to thermal decomposition. Hence, the optimum pH_i for P recovery from a nutrient-rich source is dependent on the goals of the process. Higher $pH_i \geq 10$, would be necessary if P removal is the priority. However, if maximizing the struvite content is the objective, a pH_i of 9−10 is ideal. The thermal stability is indicative of the susceptibility of the solid to decomposition, which may be useful in predicting the release of nutrients. If this property is the major concern, then a pH_i in the lower range should be considered. These observations may be complicated by additional ions in more complex waste solutions. However, these results do provide new fundamental information that can be used as a starting point in the selection of a suitable pH_i for P recovery based on the desired solid properties. In addition, this research showcases the utility of more advanced techniques such as ^{31}P NMR and TG/DSC-FT-IR in confirming the composition of the P-bearing solids and can be useful for identifying precipitates recovered from nutrient-rich wastes.

■ ASSOCIATED CONTENT

Ⓢ Supporting Information

Table S1: Saturation index (SI) of P-bearing minerals and pH before and after P precipitation. This material is available free of charge via the Internet at http://pubs.acs.org.

■ AUTHOR INFORMATION

Corresponding Author

*Email: Ashaki.Rouff@qc.cuny.edu. Phone: 718-997-3073. Fax: 718-997-3299.

Notes

The authors declare no competing financial interest.

■ ACKNOWLEDGMENTS

Support for this research was provided by the National Science Foundation under Grant No. EAR-1251732. We thank Dr. Patrick Brock for assistance with the SEM. We also thank Dr. Robert Downs and the RRUFF project for the loan of the kovdorskite mineral specimen.

Table 2. Concentrations of Evolved $H_2O(g)$ and $NH_3(g)$ per Gram of Solid Synthesized at pH_i 8−11[a]

pH_i	$H_2O(g)$ mmol/g	$NH_3(g)$ mmol/g ≤ 200 °C	$NH_3(g)$ mmol/g ≥ 200 °C	total volatiles mmol/g	$H_2O(g)$/total $NH_3(g)$	$H_2O(g)/NH_3(g)$ ≥ 200 °C
8	21.0	5.8	2.9	29.7	2.4	7.3
9	18.6	9.0	2.6	30.1	1.6	7.2
10	17.5	10.1	2.5	30.0	1.4	7.0
11	20.3	6.3	1.9	28.5	2.5	10.6

[a]Error for these measurements is ±0.11%. The $NH_3(g)$ evolved is reported for temperatures from 40−200 °C (≤ 200 °C) and 200−400 °C (≥ 200 °C). The ratio of $H_2O(g)$ to total $NH_3(g)$ (40−400 °C) and to $NH_3(g)$ evolved at 200−400 °C is determined.

REFERENCES

(1) Cordell, D.; Rosemarin, A.; Schroder, J. J.; Smit, A. L. Towards global phosphorus security: A system framework for phosphorus recovery and reuse options. *Chemosphere* **2011**, *84*, 747−758.

(2) de-Bashan, L. E.; Bashan, Y. Recent advances in removing phosphorus from wastewater and its future use as fertilizer (1997−2003). *Water Res.* **2004**, *38*, 4222−4246.

(3) Ronteltap, M.; Maurer, M.; Hausherr, R.; Gujer, W. Struvite precipitation from urine - influencing factors on particle size. *Water Res.* **2010**, *44*, 2038−2046.

(4) Suzuki, K.; Tanaka, Y.; Kuroda, K.; Hanajima, D.; Fukumoto, Y.; Yasuda, T.; Waki, M. Removal and recovery of phosphorus from swine wastewater by demonstration crystallization reactor and struvite accumulation device. *Bioresour. Technol.* **2007**, *98*, 1573−1578.

(5) Parsons, S.; Smith, J. Phosphorus removal and recovery from municipal wastewaters. *Elements* **2008**, *4*, 109−112.

(6) Manning, D. A. C. Phosphate minerals, environmental pollution and sustainable agriculture. *Elements* **2008**, *4*, 105−108.

(7) Ostara Nutrient Recovery Technologies. http://www.ostara.com.

(8) Gunn, D. J. Mechanism for the formation and growth of ionic precipitates from aqueous solution. *Faraday Discuss. Chem. Soc.* **1976**, *61*, 133−140.

(9) Nelson, N. O.; Mikkelsen, R. L.; Hesterber, D. L. Struvite precipitation in anaerobic swine lagoon liquid: effect of pH and Mg:P ratio and determination of rate constant. *Bioresour. Technol.* **2003**, *89*, 229−236.

(10) Ben Moussa, S.; Tlili, M. M.; Batis, N.; Ben Amor, M. Influence of temperature on struvite precipitation by CO_2-degassing method. *Cryst. Res. Technol.* **2011**, *46*, 255−260.

(11) Ohlinger, K. N.; Young, T. M.; Schroeder, E. D. Kinetics effects on preferential struvite accumulation in wastewater. *ASCE J. Environ. Eng.* **1999**, *125*, 730−737.

(12) Harrison, M. L.; Johns, M. J.; White, E. T.; Mehta, C. M. Growth rate kinetics for struvite crystallization. *Chem. Eng. Trans.* **2011**, *25*, 309−314.

(13) Bhuiyan, M. I. H.; Mavinic, D. S.; Beckie, R. D. Nucleation and growth kinetics of struvite in a fluidized bed reactor. *J. Cryst. Growth* **2008**, *310*, 1187−1194.

(14) Ma, N.; Rouff, A. A. Influence of pH and oxidation state on the interaction of arsenic with struvite during mineral formation. *Environ. Sci. Technol.* **2012**, *46*, 8791−8798.

(15) Abbona, F.; Calleri, M.; Ivaldi, G. Synthetic struvite, $MgNH_4PO_4.6H_2O$: Correct polarity and surface features of some complementary forms. *Acta Crystallogr.* **1984**, *B40*, 223−227.

(16) Chauhan, C. K.; Joseph, K. C.; Parekh, B. B.; Joshi, M. J. Growth and characterization of struvite crystals. *Indian J. Pure Ap. Phy.* **2008**, *46*, 507−512.

(17) Frost, R. L.; Weier, M. L.; Erickson, K. L. Thermal decomposition of struvite implications for the decomposition of kidney stones. *J. Therm. Anal. Calorim.* **2004**, *76*, 1025−1033.

(18) Abdelrazig, B. E. I.; Sharp, J. H. Phase changes on heating ammonium magnesium phosphate hydrates. *Thermochim. Acta* **1988**, *129*, 197−215.

(19) Afzal, M.; Iqbal, M.; Ahmad, H. Thermal analysis of renal stones. *J. Therm. Anal.* **1992**, *38*, 1671−1682.

(20) Rouff, A. A. The use of TG/DSC-FT-IR to assess the effect of Cr sorption on struvite stability and composition. *J. Therm. Anal. Calorim.* **2012**, *110*, 1217−1223.

(21) Stratful, I.; Scrimshaw, M. D.; Lester, J. N. Conditions influencing the precipitation of magnesium ammonium phosphate. *Water Res.* **2001**, *35*, 4191−4199.

(22) Barat, R.; Bouzas, A.; Marti, N.; Ferrer, J.; Seco, A. J. Precipitation assessment in wastewater treatment plants operated for biological nutrient removal: A case study in Murcia, Spain. *J. Environ. Manage.* **2009**, *90*, 850−857.

(23) Babic-Ivancic, V.; Kontrec, J.; Brecevic, L.; Kralj, D. Kinetics of struvite to newberyite transformation in the precipitation system $MgCl_2$−$NH_4H_2PO_4$−NaOH−H_2O. *Water Res.* **2006**, *40*, 3447−3455.

(24) Rouff, A. A. Sorption of chromium with struvite during phosphorus recovery. *Environ. Sci. Technol.* **2012**, *46*, 12493−12501.

(25) Etter, B.; Tilley, E.; Khadka, R.; Udert, K. M. Low-cost struvite production using source-separated urine in Nepal. *Water Res.* **2011**, *45*, 852−862.

(26) Le Corre, K. S. Understanding Struvite Crystallization and Recovery. Ph. D. Dissertation, Cranfield University, Cranfield, Bedfordshire, U.K., 2006.

(27) Liu, Z.; Zhao, Q.; Wei, L.; Wu, D.; Ma, L. Effect of struvite seed crystal on MAP crystallization. *J. Chem. Technol. Biotechnol.* **2011**, *86*, 1394−1398.

(28) Parkhurst, D. L.; Appelo, C. A. J. *User's Guide to PHREEQC (version 2)—A Computer Program for Speciation, Batch-Reaction, One-Dimensional Transport, and Inverse Geochemical Calculations*; Water-Resources Investigations Report 99-4259; U.S. Geological Survey: Denver, CO, 1999.

(29) Ohlinger, K. N.; Young, T. M.; Schroeder, E. D. Predicting struvite formation in digestion. *Water Res.* **1998**, *32*, 3607−3614.

(30) Boistelle, R.; Abbona, F.; Lundager Madsen, H. E. On the transformation of struvite into newberyite in aqueous systems. *Phy. Chem. Miner.* **1983**, *9*, 216−222.

(31) Kamnev, A. A.; Antonyuk, L. P.; Colina, M.; Chernyshev, A. V.; Ignatov, V. V. Investigation of a microbially produced structural modification of magnesium−ammonium orthophosphate. *Monastshefte Chem.* **1999**, *130*, 1431−1442.

(32) Shand, C. A.; Coutts, G.; Hillier, S.; Lumsdon, D. G.; Chudek, A.; Eubeler, J. Phosphorus composition of sheep feces and changes in the field determined by ^{31}P NMR spectroscopy and XRPD. *Environ. Sci. Technol.* **2005**, *39*, 9205−9210.

(33) Scrimgeour, S. N.; Chudek, J. A.; Lloyd, C. H. The determination of phosphorus containing compounds in dental casting investment products by ^{31}P solid-state MAS-NMR spectroscopy. *Dent. Mater.* **2007**, *23*, 415−424.

(34) Turner, G. L.; Smith, K. A.; Kirkpatrick, R. J.; Oldfield, E. Structure and cation effects on phosphorus-31 NMR chemical shifts and chemical-shift anisotropies of orthophosphates. *J. Magn. Reson.* **1986**, *70*, 408−415.

(35) Abbona, F.; Lundagger Madsen, H. E.; Boistelle, R. Crystallization of two magnesium phosphates, struvite and newberyite: effect of pH and concentration. *J. Cryst. Growth* **1982**, *57*, 6−14.

(36) Le Corre, K. S.; Valsami-Jones, E.; Hobbs, P.; Jefferson, B.; Parsons, S. A. Agglomeration of struvite crystals. *Water Res.* **2007**, *41*, 419−425.